Model analysis of a hammer–string interaction

Hideo Suzuki
Ono Sokki Company, Limited, Shinjuku, Tokyo 163, Japan

(Received 13 March 1985; accepted for publication 8 July 1987)

A hammer–string interaction for the bass note (A_0) of a 6-ft grand piano is investigated by use of a lumped-element model. The hammer head is simulated by a mass–spring system with a nonlinear spring characteristic. The string is simulated by many parallel resonant circuits, each of which consists of a mass, a linear spring, and a dashpot. The impulsive force applied by the hammer to the string lasts only approximately 1 ms for a hard-hit key. The string deformation at the striking point also reaches near its maximum within about this time and retains its amplitude until the wave is reflected back from the closer end at approximately 4 ms. The hammer leaves the string temporarily, since the hammer is slowly moving downward after the first impact. The string reduces its displacement rapidly when the wave is reflected back from the closer end and, consequently, it pushes the hammer farther back. Effect of hammer stiffness, hammer velocity, and inharmonicity on the spectral distribution of partials and the efficiency of energy transmission are also discussed.

PACS numbers: 43.75.Mn

INTRODUCTION

For a hard-hit key, a piano hammer is accelerated by the key action up to several meters per second at the time of contact between hammer and string. A portion of the kinetic energy of the hammer is transferred to the string within a time on the order of a millisecond. The energy stored in the string is partly transmitted to the soundboard. A portion of this energy is then radiated into the air as sound. Sound quality is determined by the harmonic content of string vibration, and the vibration and radiation characteristics of the soundboard at resonance frequencies of the string. Therefore, a better understanding of the hammer–string interaction, which determines the string vibration, is very important for improvement of piano-tone quality.

The theoretical and experimental study of the hammer–string interaction has a long history.[1] Recently, Yanagisawa *et al.*[2] assumed a coefficient of restitution between a string and a hammer and calculated the time history of the displacement of the string. Bacon and Bowsher[3] studied the vibration of a string by representing it by a finite number of particles joined together by light springs, where the hammer stiffness was neglected. Nakamura[4] represented the piano hammer by a single mass–spring system and the string by an electrical transmission line, and obtained a force-time pattern by use of an analog computer.

One common weakness of the above-mentioned studies is that the nonlinear property of the hammer head is not well taken care of. The nonlinear characteristics of hammers seem to be very important in determining the piano tone, in view of the qualitative difference of tones, as well as the loudness difference between soft-hit and hard-hit keys. Recently, Yanagisawa and Nakamura[5] measured the displacement of the string and felt deformation as a function of time and concluded that a piano hammer must be represented as a distributed mass, spring, and loss system, and emphasized the importance of the dynamic stiffness. The present author[6] developed a dynamic measurement technique of the relationship between the hammer deformation and the force applied to an ideally rigid stringlike piece. The dynamic force-displacement curve of a particular hammer is simulated by use of a model comprised of a mass and a spring with a high degree of nonlinearity.

The present article describes a new model of the hammer–string interaction and some results of numerical calculations carried out for a bass string and hard and soft hammers. The model is applied to a hammer and a string for note A_0 (key #1) of a 6-ft grand piano. The hammer and the string displacements, and the force acting between them, are discussed in detail. Effects of parameters such as hammer-head stiffness, hammer velocity, and inharmonicity on the hammer–string interaction are also discussed.

I. EQUIVALENT CIRCUIT OF A HAMMER–STRING SYSTEM

From the dynamic measurement of force-time and acceleration-time patterns of the hammer (when it hits a stringlike rigid piece), the author[6] found that the force-displacement relationship of the hammer head is approximated by the form

$$F = K_1 y^2 + K_2 y^3 + K_3 y^4, \tag{1}$$

where F is the force (applied by the hammer to the stringlike rigid piece), y is the displacement (equal to the deformation of hammer felt, in this case), and K_1, K_2, and K_3 are constants. Then the stiffness $S_h(y)$ of the hammer is given by

$$S_h(y) = F/y = K_1 y^1 + K_2 y^2 + K_3 y^3. \tag{2}$$

Because of the hysteresis characteristic, the locus of the hammer motion on the force-displacement plane takes different paths for the upward and downward motions of the hammer of a grand piano. It is assumed for simplicity, however, that the hysteresis characteristic is negligible. An important point of Eq. (1) is that a hammer head has a high degree of nonlinearity in its force-displacement relationship.

 0001-4966/87/101145-07$00.80

An equivalent hammer mass M_h is also calculated as $M_h = -F/\ddot{y}$ on the assumption that the hammer is represented by a single mass–spring system.

The differential equation of the transverse displacement $Y(x)$ of an ideal string, when driven by a sinusoidal force, is given by[7]

$$T\frac{d^2Y(x)}{dx^2} + \mu\omega^2 Y(x) = -F\delta(x - X_0), \tag{3}$$

where T is string tension, μ is string mass per unit length, ω is angular frequency, F is amplitude of the sinusoidal driving force applied at $x = X_0$, δ is Dirac's delta function, and the time-dependent term $e^{j\omega t}$ is removed. The solution of Eq. (3) is expressed as a summation of individual eigenfunctions by use of the boundary conditions ($Y = 0$) as

$$Y_{\mathbb{R}}(x) = \sum_{n=1}^{\infty} \frac{A_n \sin(n\pi x/L)}{\sin(n\pi X_0/L)}, \tag{4}$$

with the coefficients,

$$A_n = F\sin^2(n\pi X_0/L)/[T(n\pi/L)^2 - \mu\omega^2]L/2. \tag{5}$$

Equations (4) and (5) indicate that the driving-point impedance at $x = X_0$ for the nth mode is the same as that of a resonant system with mass M_n and stiffness S_n in series

$$M_n = \mu L/[2\sin^2(n\pi X_0/L)] \tag{6}$$

and

$$S_n = \mathbb{R}[(n\pi/L)^2(T/\mu)M_n], \tag{7}$$

where M_n and S_n are considered as the nth modal mass and stiffness of the string at the driving point at $x = X_0$. The resonance angular frequency of the nth mode of a flexible string is given by

$$\omega_n = (n\pi/L)(T/\mu)^{1/2}. \tag{8}$$

It can be seen that the total driving-point impedance of the string is the same as that of a parallel connection of an infinite number of resonant circuits[8] with M_n and S_n ($= 1/C_n$).

In the above discussion, the damping of the string is neglected. The main cause of the damping in a practical situation is the finite impedance at the bridge. The energy stored in the string gradually leaks to the soundboard through the bridge. The decay of string motion is taken care of here by addition of the resistors R_n in each resonant branch.

A similar procedure can be followed even if it is necessary to take into consideration the effect of the string stiffness. Modifications of the eigenfunctions and the boundary conditions are necessary in this case. This may cause slight changes of the equivalent masses, the stiffnesses, and the resonance frequencies. Probably the most important effect of the string stiffness is to increase the resonance frequencies of higher orders from those given by Eq. (8). In this article, it is assumed that the partials satisfy the inharmonic relationship[9]

$$f_n/f_1 = n[(1 + Bn^2)/(1 + B)]^{1/2}, \tag{9}$$

where f_n is the nth partial frequency and B is the inharmonicity index. Only the stiffness given by Eq. (7) is modified so that the inharmonicity relationship of Eq. (9) holds. The modification is achieved simply by multiplying S_n of Eq. (7) by $(f_n/nf_1)^2$. The physical implication of this modification is that the higher frequency components travel faster than the lower frequency components.

By combining the two models described above, the author obtained the equivalent circuit of the hammer–string system shown in Fig. 1. In the impedance analogy, the mass and the compliance (inverse of stiffness of the hammer) correspond to the inductor and the capacitor, respectively. Also, the force and the displacement correspond to the voltage and the charge, respectively. The hammer is accelerated by the key action to initial velocity V_h just before it hits the string. This phenomenon is analogous to a current induced by a voltage source (which is not shown in the model, since the hammer is freed from acceleration at the time of contact). Switch SW indicates the contact or noncontact state between the hammer and the string. The current keeps running in the closed loop without charging the capacitor C_h until switch SW is opened. Once it is opened, capacitor C_h starts being charged and, at the same time, current starts running into the resonant branches. The displacement of the hammer, the deformation of the hammer felt, and the displacement of the string at the striking point are y_0, $(y_0 - y_1)$, and y_1, respectively. When $(y_0 - y_1)$ becomes negative, S_h is set equal to zero.

From the equivalent circuit, differential equations governing the behavior of the hammer–string action are obtained.

$$M_h\ddot{y}_0 + S_h(y_0 - y_1) = -M_h G, \tag{10}$$

$$S_h(y_1 - y_0) + M_1(\ddot{y}_1 - \ddot{y}_2) + R_1(\dot{y}_1 - \dot{y}_2) + S_1(y_1 - y_2) = 0, \tag{11}$$

$$\vdots$$

$$M_{n-1}(\ddot{y}_N - \ddot{y}_{N-1}) + R_{N-1}(\dot{y}_N - \dot{y}_{N-1}) + S_{N-1}(y_N - y_{N-1}) + M_N\ddot{y}_N + R_N\dot{y}_N + S_N y_N = 0, \tag{12}$$

where G is the constant of gravitation and the highest order of mode is N. The effect of the gravity is considered only on the motion of the hammer.

In order to solve the $(N + 1)$ simultaneous differential equations, the continuous time functions are discretized. The notation $y(m)$ means the value of $y(t)$ at $t = m\Delta t$, where m is an integer and Δt is the time interval of discretization. Then, the time derivatives $\dot{y}(m)$ and $\ddot{y}(m)$ are approximated by

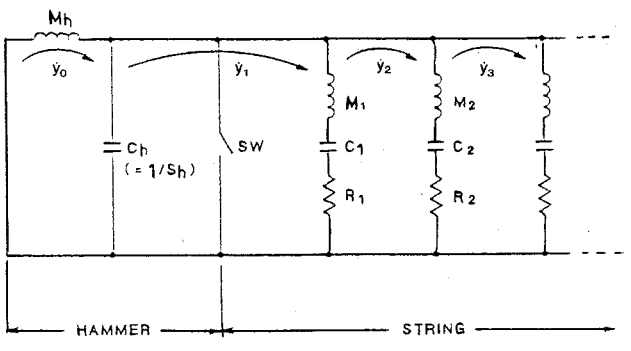

FIG. 1. Hammer–string interaction model.

$$\dot{y}(m) = [y(m+1) - y(m-1)]/2\Delta t \tag{13}$$

and

$$\ddot{y}(m) = [y(m+1) - 2y(m) + y(m-1)]/(\Delta t)^2, \tag{14}$$

respectively. Applying Eqs. (13) and (14) to Eq. (12), we obtain $(N+1)$ equations of the following form:

$$\{y(m+1)\} = \{y_G\} + [A]\{y(m)\} + [B]\{y(m-1)\}, \tag{15}$$

where $[A]$ and $[B]$ are $(N+1)\times(N+1)$ rectangular matrices, and $\{y(i)\}$ $[i=(m-1), m, (m+1)]$ are the displacement vectors, and $\{X_G\}$ is the displacement vector representing the effect of gravity. The nonlinear term S_h is included only in $[A]$, which must be revised for different values of hammer deformation. Equation (15) shows that if we know the vectors $\{y(m-1)\}$ and $\{y(m)\}$, we can determine the vector $\{y(m+1)\}$. The initial conditions are

$$\{y(0)\} = \{0,0,...,0\}^T. \tag{16}$$

and

$$\{y(-1)\} = \{-V_h\Delta t,0,0,...,0\}^T. \tag{17}$$

Using Eqs. (15)–(17), the time history of the hammer and the string is obtained for $t = m\Delta t$, where $m = 1,2,\ldots$.

II. RESULTS AND DISCUSSION

There are many parameters that affect the interaction between the hammer and the string. Primary values of those parameters chosen for the calculation are shown in Table I. Experimentally obtained values for a bass hammer are used. The mass M_h is 11 g, hammer stiffness coefficients K_1, K_2, and K_3 are -2.0 (N/mm^2), 6.2 (N/mm^3), and 52.4 (N/mm^4), respectively. The initial hammer velocity V_h for the primary case is chosen to be 3 m/s.

The dimensions of the string and the ratio of the length from the striking point to the closer end (X_0) to the speaking length of the string (L) were obtained by measuring a string of note A_0 of a style "L" Steinway piano. The primary values of the mass per unit length (0.18 kg/m) and the inharmonicity index (4.4×10^{-4}) are of the order of magnitudes observed experimentally. The quality factor Q_n of the string resonance was roughly estimated from measured decay rates of partials. In any case, due to the large quality factors, the effect of the damping on the hammer–string interaction is negligible. The order of the highest partial N is 50. The result did not change significantly even if N was increased to 60. If N is not large enough, however, the string becomes effectively stiffer and the period of contact becomes shorter.

TABLE I. Primary parameters of the model.

Hammer	Mass	M_h(g)	11
	Stiffness coefficients	$K_1(N/\text{mm}^2)$	-2.0
		$K_2(N/\text{mm}^3)$	6.2
		$K_3(N/\text{mm}^4)$	52.4
	Velocity	V_h(m/s)	3
String	Length	L(m)	1.28
	Linear mass	μ(kg/m)	0.18
	Inharmonicity index	B	4.4×10^{-4}
	Striking point ratio	X_0/L	0.115
	Quality factor	Q_n	$400n$

A. Time history of hammer and string displacements and force acting on the string

The force-time pattern of the hammer acting on the string, and the displacement-time patterns of the hammer and of the string at the striking point are shown in Fig. 2 for the primary case. The interaction lasts approximately 6.5 ms for this case. The displacement curve of the hammer during the interaction is represented by three straight lines. Accordingly, the interaction may be categorized into three stages. During the first stage, the main excitation of the string occurs due to a large impulsive force applied to the string. At the beginning of the second stage, the string displacement at the driving point is already close to its maximum, and the hammer is moving downward slowly. Since the deformation of the hammer is small, the reacting force between the hammer and the string is almost negligible. At the end of this stage, a temporary loss of contact is observed. During the last stage, the hammer is accelerated downward by the string when the reflected wave from the shorter end returns to the striking point. A portion of energy stored in the string in the first stage is fed back to the hammer in this stage, reducing the efficiency of energy transmission.

It is encouraging that the present results are similar to the experimental results shown in Ref. 5, for the same note and an approximate hammer velocity of 2 ms, even though the parameters used for the present model are probably different from those of the piano used for their study. The duration of the interaction is approximately 7 ms for their case. The displacement-time patterns of the strings are very similar to each other. The string amplitude in the present case is roughly 1.5 times larger than that of Ref. 5. The force-time pattern of the present model is also very similar to that of Ref. 5.

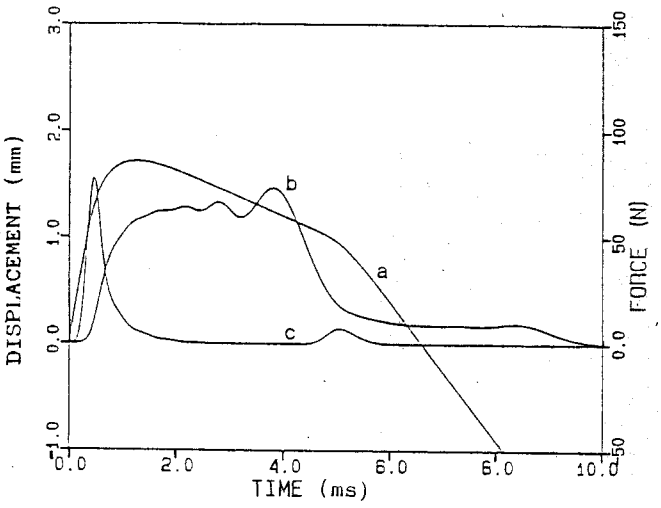

FIG. 2. Time histories of (a) hammer displacement, (b) string displacement at the striking point, and (c) force of the hard hammer acting on the string (right-hand scale) for the primary parameters, including hammer velocity $V_h = 3$ m/s.

Figure 2 shows that approximately 4 ms after the start of contact the string displacement is greater than that of the hammer, resulting in a temporary loss of contact. This time is roughly equal to the time needed for the transverse wave to propagate from the striking point to the closer end and back again to the striking point. Since the hammer is already moving downward and the string displacement stays approximately the same during the second stage, the hammer eventually leaves the string. If the wave reflected from the closer end reaches the striking point early enough, the string displacement reduces suddenly, and the string catches up with the hammer and the "recontact" occurs. The temporary loss-of-contact phenomenon may be understood more clearly by looking at the deflections of the whole string at different times during the first 10 ms. They are shown in Fig. 3. The width of the string deflection increases until its left front reaches the closer end. After the reflection, the wave of the string deflection moves to the right with an approximately constant width. Because of the slightly negative deflection at the left front, the string deflection shows a hump at its end after the reflection. The loss-of-contact and recontact phenomenon occurs when the rear edge of the main wave reaches the striking point. This phenomenon seems to be very common for the bass hammer–string interaction.

Another interesting thing seen in Fig. 3 is that small ripples precede the main wave. This is caused by the inharmonicity or, in other words, by the larger transverse wave velocities of the higher-order partials. The effect of the inharmonicity is discussed in more detail in Sec. II D.

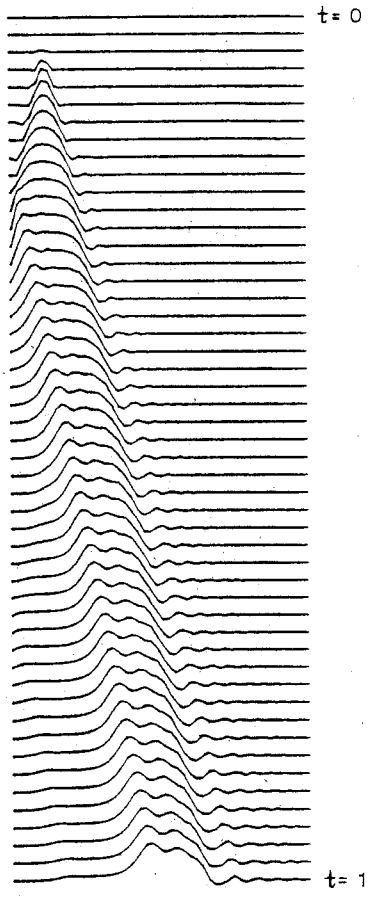

FIG. 3. Deformation of the string at 0.2-ms intervals over the first 10 ms for the primary case.

B. Hammer-head stiffness

It is a very common practice to increase the hammer stiffness in order to brighten the tone quality. However, this is not the only result obtained by increasing the stiffness. The time histories of the hammer and string displacements and the force acting between them for the case of a soft hammer ($K_1 = -15.6$, $K_2 = 26.1$, $K_3 = 7.5$) are shown in Fig. 4. Other parameters are the same as the primary case. The string displacement-time pattern at the driving point is smoother than the primary case, indicating that the amplitude of the string vibration has smaller components of higher-order partials than the standard case. This is seen more clearly by considering the relative magnitudes of vertical forces F_n applied by the string to the farther end (to the bridge of a real piano). Since it determines the slope of the string at both ends, each vertical force is calculated for each partial mode.

Force level $20 \log|F_n/F_0|$ in decibels is plotted in Fig. 5, as a function of partial mode order n, F_0 being an arbitrarily chosen reference force. With m a positive integer, a force level of order $9m$ is relatively small, because the driving point is close to a node of the $9m$th partial mode. For this lowest bass string A_0 of a grand piano, for partial modes up to 15, force levels for the soft hammer (line with dots in Fig. 5) are relatively greater than force levels for the hard hammer. For higher-numbered partial modes, force levels for the hard hammer are relatively greater than force levels for the soft hammer.

C. Hammer velocity

Since the system is nonlinear, the behavior of the hammer and the string is different for different hammer velocities. The hammer and the string displacements and the force patterns for the hammer velocity at 1 m/s are shown in Fig. 6. Other parameters are the same as the primary case. A

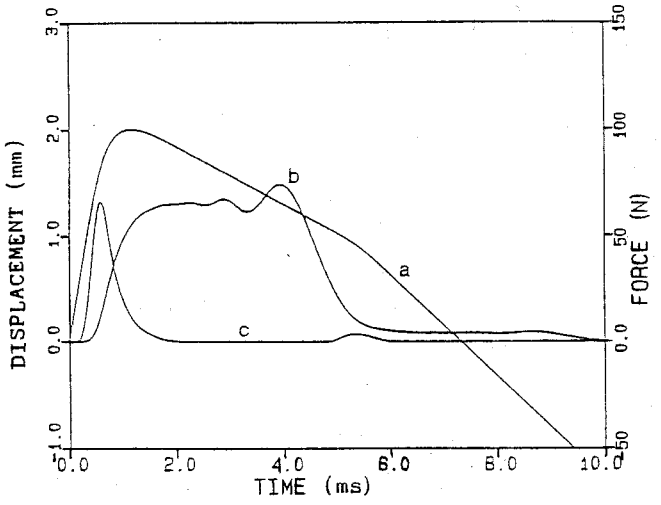

FIG. 4. For a soft hammer, time histories of (a) hammer displacement, (b) string displacement at the striking point, and (c) force of the hammer acting on the string (right-hand scale). Other parameters are for the primary case.

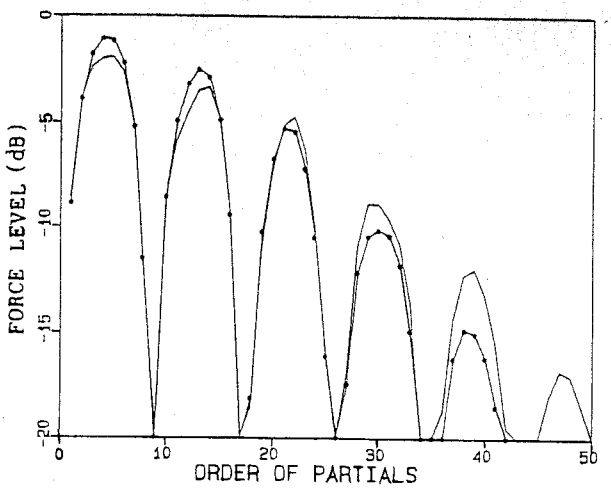

FIG. 5. Force level spectra of partials for the hard hammer (solid line) and the soft hammer (line with dots).

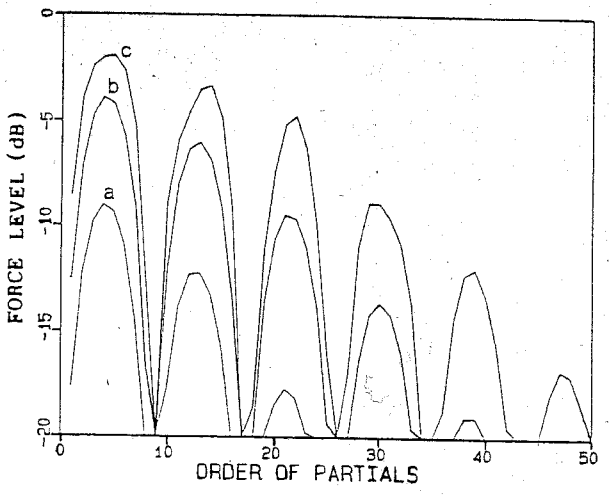

FIG. 7. Force level spectra of partials for (a) $V_h = 1$ m/s, (b) 2 m/s, and (c) 3 m/s.

significant difference between these two results (Figs. 2 and 6) is seen in their force-time patterns. For $V_h = 3$ m/s, the major force applied to the string is narrower and larger compared to the case for $V_h = 1$ m/s. This results in high-frequency components of the string vibration for the case with $V_h = 3$ m/s. The dependence of the force spectra of the partials on the hammer velocity is shown in Fig. 7. It is clearly seen that the force spectra of the higher orders increase more rapidly than the lower orders do when the hammer velocity is increased. This is a quantitative explanation of why a piano tone sounds brighter, as well as louder, when a key is hit harder,

The efficiency of the energy transmission from the hammer to the string is also affected significantly by the hammer velocity. The efficiency of energy transmission η is defined as

$$\eta = 1 - (V_h'/V_h)^2, \tag{18}$$

where V_h' is the hammer velocity at the end of the interaction. Figure 8 shows the results for hard and soft hammers for different hammer velocities. In general, the efficiency is very high except for very small hammer velocities. The efficiency is low for small hammer velocity, since the hammer impedance is effectively lower than the driving point impedance of the string. As the hammer velocity increases, the hammer becomes stiffer and the efficiency is increased. Notice that the third stage described in Sec. II A is missing for $V_h = 1$ m/s. When the hammer velocity is increased more, the third stage starts to appear and the portion of the energy stored in the string is transmitted back to the hammer causing the reduction of energy transmission. For a softer hammer, a larger hammer velocity is required to reach the maximum efficiency.

D. Inharmonicity

In the preceding sections, it was assumed that the frequencies of the partials satisfy the inharmonicity relationship given by Eq. (9), i.e., that the wave propagation of the

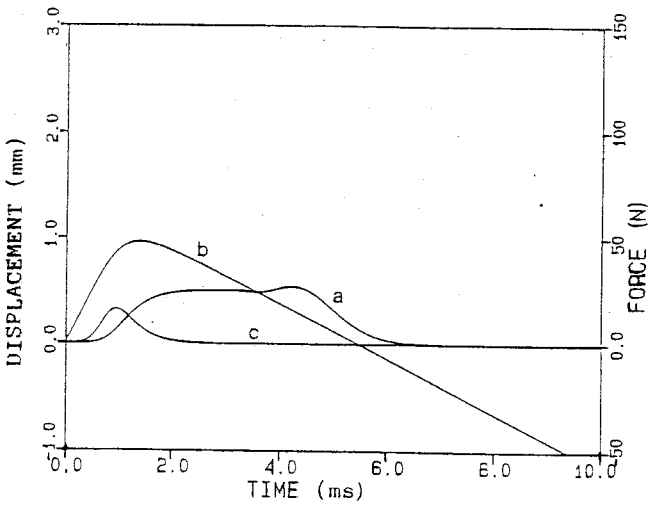

FIG. 6. For hammer velocity $V_h = 1$ m/s, time histories of (a) hammer displacement, (b) string displacement at the striking point, and (c) force of the hammer acting on the string (right-hand scale). Other parameters are for the primary case.

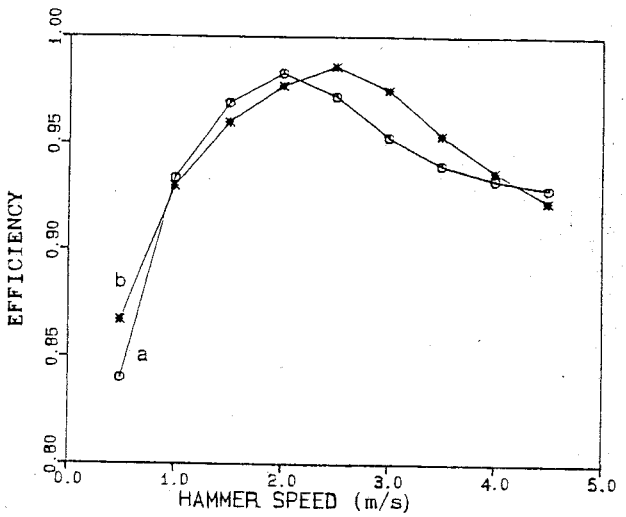

FIG. 8. Efficiency of energy transmission for (a) the hard hammer and (b) the soft hammer.

present string is dispersive. The results are compared with those of the harmonic case in order to find out the effect of the inharmonicity.

Figure 9 shows the time history of the hammer–string interaction of an ideally flexible string, i.e., for inharmonicity index $B = 0$. A significant difference between the present case and the primary case is that the width of the string deformation is more clearly defined for the harmonic case. This causes a difference between the force-time patterns of the two cases. Since the slope of the hammer displacement at the third stage for the harmonic case is smaller than for the primary case, the energy transmission is more effective for the harmonic case.

The dispersive nature of the string vibration with inharmonicity will be clearly seen by comparing the wave propagation for the harmonic case, which is shown in Fig. 10, with that of the inharmonic case (Fig. 3). The sharp front of the wave is maintained all the time for the harmonic case, whereas that of the inharmonic case becomes less steep as the time passes. The force spectra of the harmonics and of the partials are also different. Those are compared in Fig. 11. The spectra for the present case are larger for most of the orders and especially for the orders above 35. This agrees with the higher efficiency of energy transmission of the harmonic case.

III. CONCLUSION

A model simulating a hammer–string interaction is presented. The hammer is modeled as a mass–spring system. The nonlinear spring characteristic of the hammer is approximated as a function of felt deformation by use of three coefficients for polynomials of orders from 1 to 3. The string is modeled by a large number of resonant circuits connected in parallel. The effect of the inharmonicity is taken care of by gradually increasing the resonance frequencies of the string as the order is increased.

The time histories of the hammer position, the string displacement at the striking point, and the force acting between the hammer and the string were discussed. The string displacement at the striking point reaches roughly its maximum after the initial impact by the hammer, and retains its amplitude until a reflected wave returns from the closer end. Since the hammer is moving downward slowly after the initial impact, it will be pushed farther downward by the string when the reflected wave comes back and the string displacement is reduced very quickly. In some cases, a temporary loss-of-contact phenomenon is observed when the first reflected wave returns to the striking point.

A hammer with a smaller stiffness excites a string with

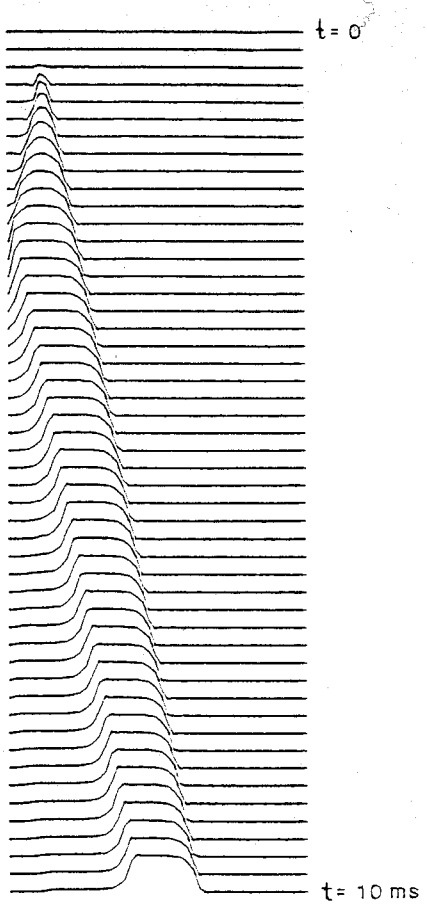

FIG. 10. Deformation of an ideal string ($B = 0$) at 0.2-ms intervals over the first 10 ms. Other parameters are for the primary case.

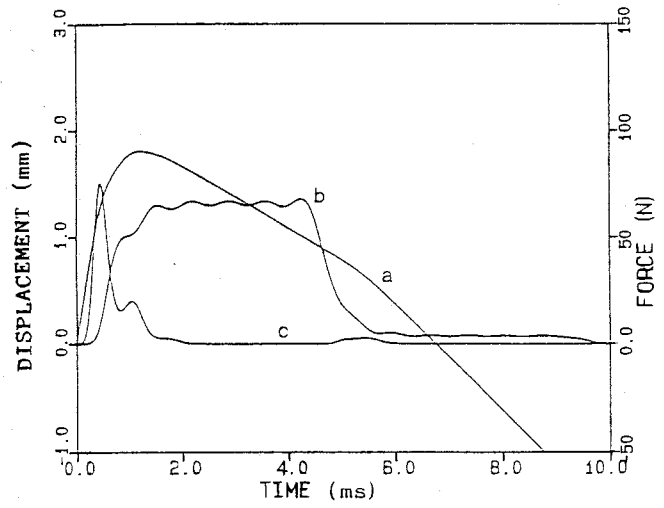

FIG. 9. For an ideal string of inharmonicity index $B = 0$, time histories of (a) hammer displacement, (b) string displacement at the striking point, and (c) force of the hammer acting on the string (right-hand scale).

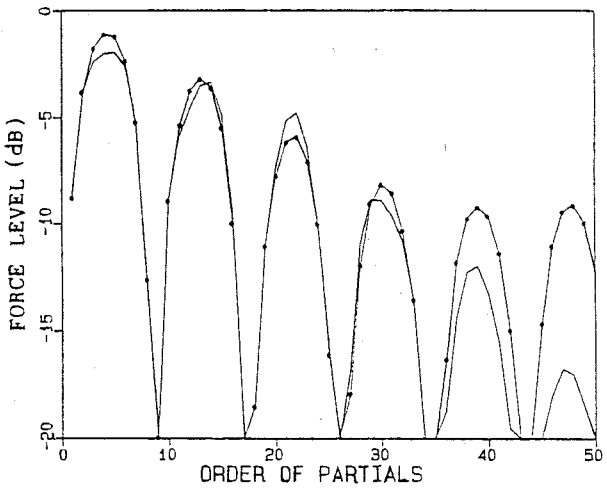

FIG. 11. Force level spectra of partials for the inharmonic case (solid line) and the harmonic case (line with dots).

larger amplitudes for lower-order partials (below 15 for the present case) and with smaller amplitudes for higher-order partials. The significance of the spectral difference of the partials can be evaluated subjectively by listening to the sound of the digital-to-analog converted signals through a loudspeaker or a piano soundboard with a shaker.

The effect of the initial hammer velocity V_h on the hammer–string interaction is remarkable. Since the hammer is effectively stiffer for a larger V_h, the spectra of higher-order partials rise faster than those of the lower-order partials as V_h is increased. The efficiency of the energy transfer is also affected by V_h. For a soft-hit key, the hammer is effectively soft and the energy is not transmitted efficiently. For a larger V_h, the energy transmission becomes more efficient. When V_h is increased farther, the string starts to push back the hammer near the end of the interaction, reducing the efficiency of energy transmission. For a softer hammer, the efficiency maximum occurs at a larger V_h. The maximum efficiency was more than 0.98 for both soft and hard model hammers used for the study.

The inharmonicity of partials considerably affects the hammer–string interaction. The efficiency of energy transfer, as well as the spectra of the partials is different between the harmonic and the inharmonic cases. Of course, the wave propagation is dispersive for the inharmonic case. A subjective evaluation of the computer-generated force signals through a loudspeaker showed that the sound for the inharmonic case was more natural.

ACKNOWLEDGMENTS

This study was conducted while the author was at CBS Technology Center in Stamford, CT, from 1981 to 1985. The author would like to acknowledge the helpful daily discussions he had with his colleagues, Gordon Ebitt and William Strong. The author would also like to thank the encouragement given by Robert Finger and Emil Torick, Directors of CBS Technology Center, in pursuing this project. He further wants to express his gratitude to Nanami Konami at Ono Sokki Co., Ltd., Japan, for her typing and editorial work.

[1] I. Nakamura, "A review of acoustical research on pianos," J. Acoust. Soc. Jpn. **35**, 447–455 (1979) (in Japanese).

[2] T. Yanagisawa, K. Nakamura, and I. Shirayanagi, "Vibration analysis of piano string and soundboard by finite element method," J. Acoust. Soc. Jpn. **31**, 661–666 (1975) (in Japanese).

[3] R. A. Bacon and J. M. Bowsher, "A discrete model of a struck string," Acustica **41**, 21–27 (1978).

[4] I. Nakamura, "The vibration of a struck string: Acoustical research on the piano, Part I," J. Acoust. Soc. Jpn. **36**, 504–512 (1980) (in Japanese).

[5] T. Yanagisawa and K. Nakamura, "Dynamic compression characteristics of piano felt," J. Acoust. Soc. Jpn. **40**, 725–729 (1984) (in Japanese).

[6] H. Suzuki, "Modeling of a piano hammer," J. Acoust. Soc. Am. Suppl. 1 **78**, S33 (1985).

[7] P. M. Morse and K. U. Ingard, *Theoretical Acoustics* (McGraw-Hill, New York, 1968), pp. 166–169.

[8] L. E. Kinsler and A. R. Frey, *Fundamentals of Acoustics* (Wiley, New York, 1962), pp. 187–213.

[9] R. W. Young, "Inharmonicity of plain wire piano strings," J. Acoust. Soc. Am. **24**, 267–273 (1952).